J. Fluid Mech. (1988), *vol.* 187, *pp.* 409–433
Printed in Great Britain

Mathematical and physical modelling of double-diffusive convection of aqueous solutions crystallizing at a vertical wall

By MOLLIE E. THOMPSON AND JULIAN SZEKELY
Department of Materials Science and Engineering, Massachusetts Institute of Technology, Cambridge, MA 02139, USA

(Received 2 July 1986 and in revised form 4 August 1987)

Solidification of a double-diffusive liquid from a vertical wall in a rectangular cavity is investigated using both mathematical and physical modelling. A two-dimensional mathematical model is developed to simulate the process of solidification in a two-component liquid containing a denser solute. Observations on the solidification behaviour of aqueous sodium carbonate solutions are used to verify the results of the mathematical analysis. The theory and experiments provide a clear picture of the role of double-diffusion in producing vertical compositional and density stratification in an initially homogeneous liquid during solidification. The development of horizontally oriented convection cells in the stratified liquid is correlated with the magnitude of the destabilizing lateral temperature difference across the liquid region.

1. Introduction

Double-diffusive phenomena have characteristically been associated with convective processes in oceanic environments. The adjective 'double-diffusive' refers to the fact that these fluid motions are generated by the interactive effect of gradients in two diffusing components, each of which contributes to the buoyancy force acting on the fluid.

One type of double-diffusive convective instability, observed both experimentally and in certain oceanic situations, occurs when a fluid exhibiting a stable vertical salinity gradient is subject to a destabilizing temperature gradient. If the destabilizing gradient is horizontal, the resultant fluid motion occurs in a series of low-aspect-ratio convection cells, stacked vertically upon one another. Double-diffusive instabilities of this type are thought to influence the development of layered or 'step-like' vertical salinity and temperature gradients observed in certain regions of the oceans.

For comprehensive review of the literature on double-diffusive phenomena the reader is referred to the excellent papers by Turner (1974, 1979) and Huppert & Turner (1981). The following discussion is therefore restricted to an overview of previous investigations of double-diffusion that are concerned with lateral heating/cooling of a stable, vertical salinity gradient.

The behaviour of a stratified fluid contained between two rigid, impermeable vertical boundaries, subject to horizontal temperature gradients, has been studied both theoretically and experimentally. Thorpe, Hutt & Soulsby (1969), Hart (1971) and Chen (1974) use stability analysis to determine the critical Rayleigh number

R_c for the onset of double-diffusive layered convection and to provide information on the general characteristics of the resultant flow patterns. Physical modelling of double-diffusive systems using salt-water and sugar–salt solutions gives results in general agreement with the stability analyses, indicating a value for R_c on the order of 1.5×10^4 (Chen 1974; Chen, Briggs & Wirtz 1971; Wirtz, Briggs & Chen 1972).

Wirtz *et al.* (1972) use numerical methods to calculate the double-diffusive flow patterns for the specific case of a narrow cavity. The results show that at Rayleigh numbers above critical, a series of double-diffusive layers are generated simultaneously along the vertical boundaries and propagate across the width of the gap. The layered structure that develops consists of horizontal convection cells separated by diffusive interfaces, and is characterized by 'stepwise' temperature and salinity profiles.

A related phenomenon, which is relevant to problems in geology, metallurgy and crystal growth, concerns the development of double-diffusive instabilities in the presence of a moving solidification/melting front. This situation differs from the classical case of double-diffusion (in the oceans) in that the liquid is initially uniform in composition and the solute gradients and associated convective instabilities in the liquid develop as a result of the solidification process.

Chen & Turner (1980), Huppert & Turner (1980) and Turner (1980) conducted experiments with salt-water and salt–sugar systems to determine the effect of crystallization on double-diffusion in simulations of mineral layering in igneous intrusions and of melting of icebergs. These investigative experiments encompass a wide range of heating and cooling configurations but consider only the situation of a liquid with a pre-existing (linear) salinity stratification.

McBirney (1980), Turner & Gustafson (1981) and McBirney, Baker & Nilson (1985) extended this physical modelling to address the problem of crystallization from a homogeneous fluid. For the experimental systems investigated, the solute-rich liquid produced upon solidification is less dense and ascends along the solid/liquid interface to the top of the cavity, creating a region with a stable, vertical concentration gradient. The lateral temperature gradient produces a series of double-diffusive convective layers within this region of the liquid, which are similar to those observed in double-diffusion experiments between vertical, impermeable boundaries.

Previous studies of solidification in double-diffusive systems, involving both uniform and non-uniform initial solute distributions, have mainly been restricted to experimental investigations. To the best of our knowledge there has been no attempt to apply numerical methods to the study of horizontal solidification in these systems, although these techniques have been used successfully in the analysis of vertical solidification problems (McFadden *et al.* 1984; Coriell, Cordes & Boettinger 1980; Brown, Chang & Adornato 1984). Furthermore, none of the existing investigations have been concerned with solidification that produces a denser, solute-rich liquid.

In this paper we present the results of both numerical and physical modelling of horizontal solidification in a double-diffusive system. During the early stages of solidification, the analysis focuses on the process by which concentration gradients develop in an initially homogeneous liquid. As solidification progresses and the magnitude of these gradients increases, the emphasis is on the role of double-diffusive phenomena in altering the transport processes and solidification behaviour of the system.

The solidification experiments with aqueous sodium carbonate solutions are described in §2. The mathematical formulation and results of the numerical

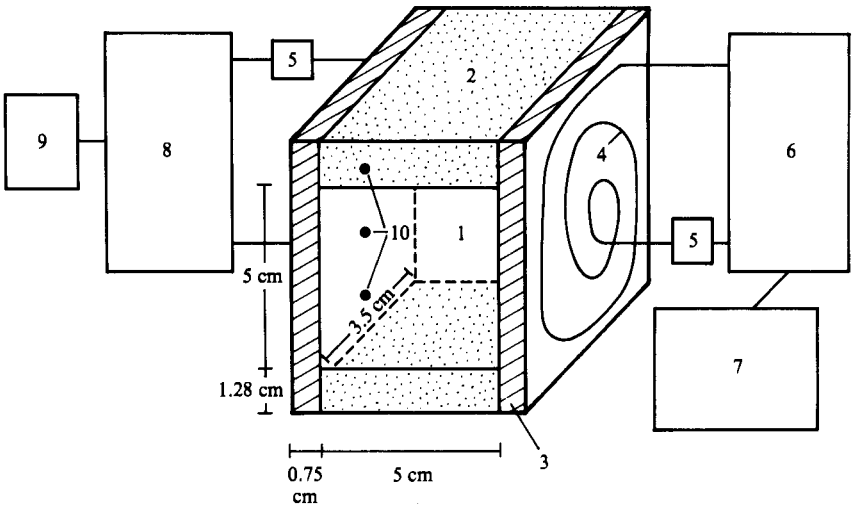

FIGURE 1. Schematic diagram of the experimental apparatus used for the study of the soldification behaviour of sodium carbonate solutions. (1) Plexiglas cavity of inner dimensions $5 \times 5 \times 3.5$ cm, (2) 1.28 cm thick Plexiglas based and removable lid, (3) 0.75 cm thick copper sidewalls, (4) tubing embedded in sideplates for circulation of coolant, (5) variable-flow-rate circulation pumps, (6) cold-temperature reservoir (methanol), (7) adjustable-temperature refrigeration unit, (8) hot/room-temperature reservoir (water), (9) immersion heater, (10) schematic location of thermocouples along vertical walls (also on cold wall).

calculations are presented and compared to the experiments in §3. In §4 the results of the previous sections are used to analyse the mechanisms by which double-diffusive instabilities develop and propagate through the system.

2. Experimental results

The role of double-diffusion in controlling transport processes during solidification is investigated experimentally using aqueous solutions of sodium carbonate. A schematic diagram of the experimental apparatus is shown in figure 1. It consists of a Plexiglas box (5 cm × 5 cm × 3.5 cm) fitted with copper sidewalls and 1.28 cm thick insulated Plexiglas lid and base designed to approach the conditions of the ideal (perfectly thermally insulating) boundaries assumed in the theoretical representation. The limited dimensions of the container (5 cm) ensure laminar flow conditions, making it possible to compare the calculated and experimental results, without requiring that the numerical calculations involve the use of a complex turbulent-flow model.

Precooled methanol at a temperature of -20 °C and preheated water circulate through tubing embedded in the cold and hot walls, respectively. Thermocouples located at three elevations along the copper plates indicated that the inner surfaces of the cold and hot walls were maintained at approximately constant temperatures of -10 and $+15$ °C (± 2 °C) respectively during the experiments. The apparatus is surrounded by 8 cm thick styrofoam insulation which is removed for observation of the solid/liquid interface and flow field. The experiments have been restricted to solutions containing less than 6 wt% sodium carbonate (eutectic composition). For these concentrations, ice is the solid phase forming throughout the majority of solidification and the solute-rich liquid has a higher density than the bulk liquid.

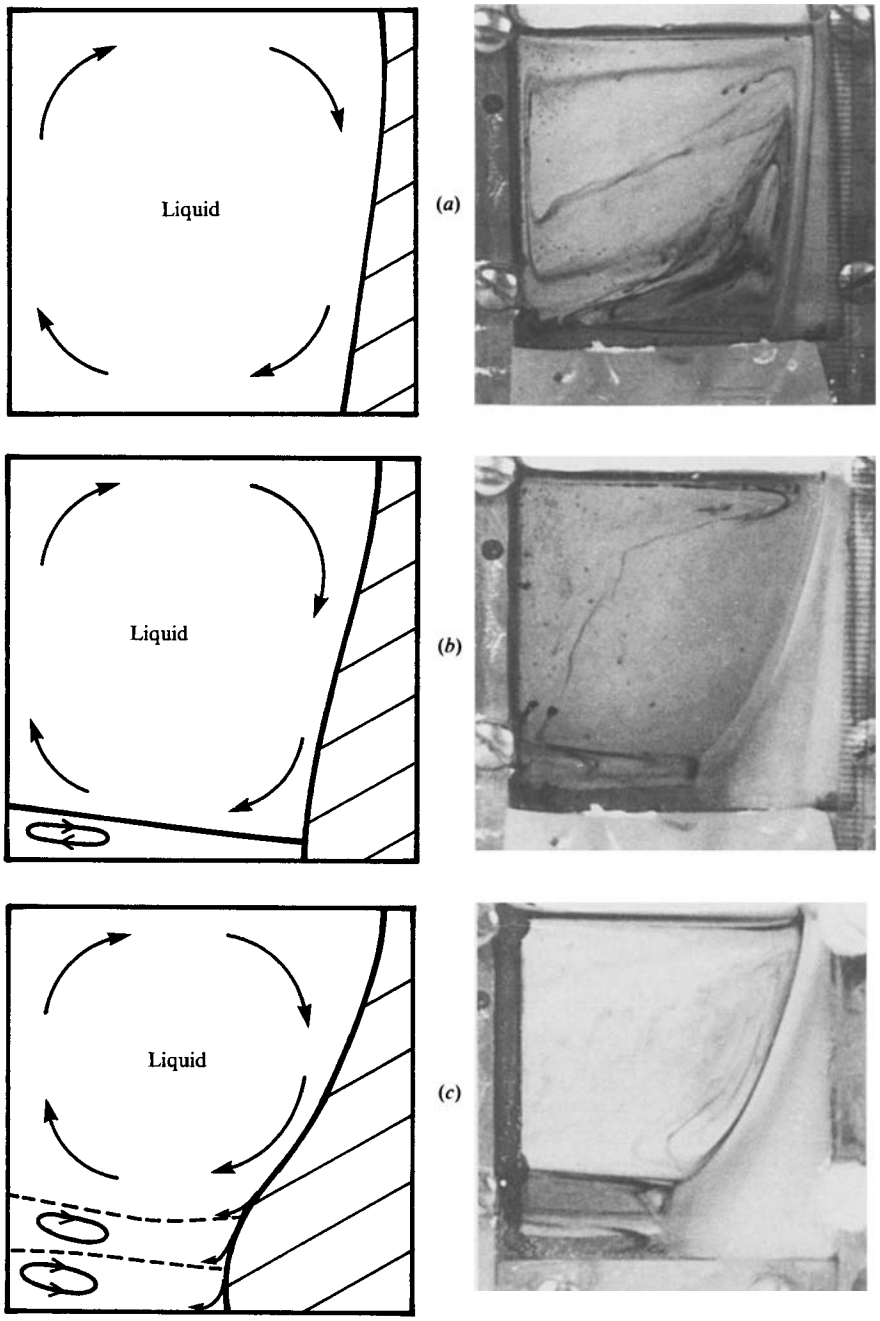

FIGURE 2(a–c). For caption see facing page.

Figure 2(a–e) shows photographs taken during the solidification of a 2 wt% sodium carbonate solution. A small amount of dye was injected into the liquid before each photograph to reveal the flow field. During the initial stages of solidification the liquid circulates in a single convection cell and the solid/liquid interface has almost a constant slope (figure 2a) with the maximum width of the solidified region occurring at the base.

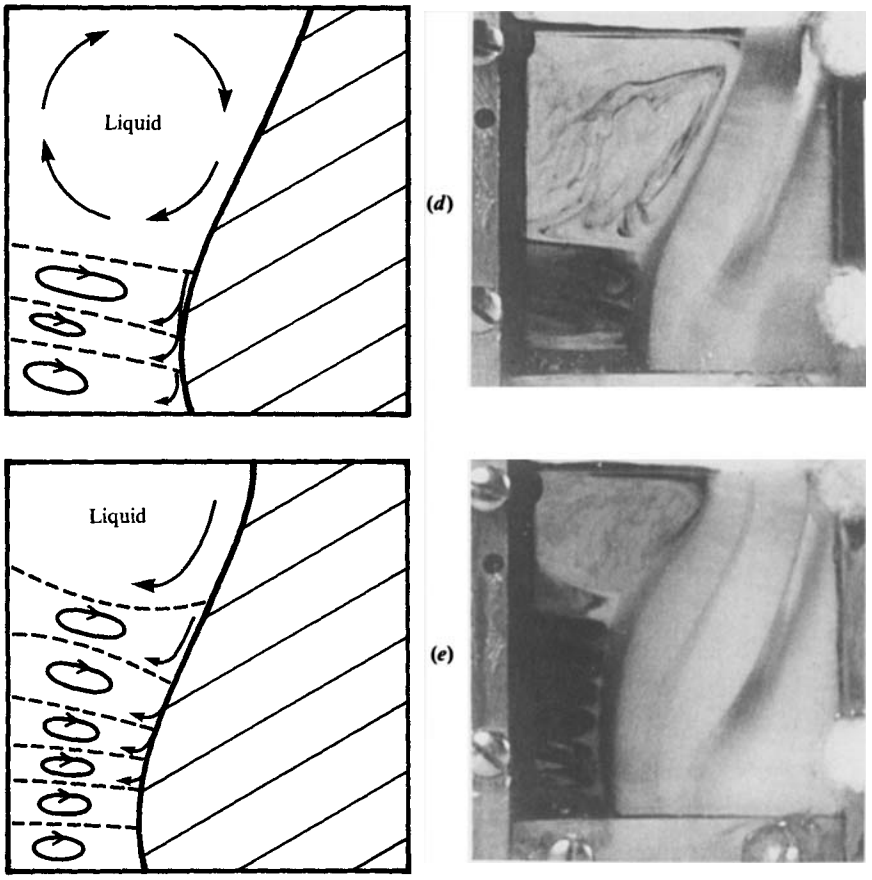

FIGURE 2. Photographs and accompanying schematic interpretations of the solidification of a 2 wt% Na_2CO_3 solution showing the evolution of the flow patterns and the position of the solid/liquid interface at a series of times after the beginning of solidification. The direction of solidification is from right to left and the solid phase forming is ice (primarily). (*a*) At this early stage (10 min) the liquid circulates in a single thermally driven convection cell and the solid/liquid interface slopes out near the base where the thermal boundary layer is thickest. (*b*) After 30 min a horizontal double-diffusive convection layer has formed beneath the main thermal convection cell, rotating in the same direction, but less vigorously than the overlying cell. (*c*) After 40 min two shallow, double-diffusive layers each ~ 0.6 cm high, have formed at the base. The solid/liquid interface is more nearly vertical in the lower region adjacent to these layers, reflecting the less vigorous circulation characteristic of the lower region. (*d*) After 1 h and 15 min the accumulation of solute-rich dense liquid at the base of the cavity creates stagnant regions above and below the double-diffusive convection layers. These regions mark the sights where additional horizontal layers will form as the cavity continues to solidify. (*e*) After 2 h and 30 min the cavity is close to 72% solidified and the original thermal convection cell is restricted to the uppermost portion of the liquid. There is evidence of between 6 and 8 shallow double-diffusive convection cells beneath this thermal cell, in which the convective motion is comparatively slow.

The solute-enriched liquid produced upon solidification is transported along the crystal/liquid interface to the base of the cavity where, owing to its relatively high density, it collects to form a separate, stable layer beneath the main convection cell. The fractionated fluid released to the boundary layer becomes increasingly enriched in solute, and therefore denser, as solidification progresses. The enriched liquid accumulates at the base in a manner analogous to the 'box-filling' process described

by Baines & Turner (1969), creating a density-stabilized region with a pronounced vertical solute concentration gradient.

Within 30 minutes the combination of the vertical (stable) solute gradient and the lateral temperature gradient, causes a low-aspect-ratio horizontal convection cell (< 1 cm high) to form within this density-stratified region, rotating in the same direction as, but more slowly than, the upper cell (figure 2*b*).

The vertical compositional boundary layer along the crystals supplies denser liquid to the base of the cavity, causing continued growth of the lower, stratified zone at the expense of the main convection cell. As the boundary layer descends through the density-stratified liquid at the base of the cavity, the outer portions are observed to 'spill off' horizontally into the interior at roughly their own density levels, thereby enhancing the density stratification. The primary channels along which the boundary-layer fluid is transported into the interior occur at the cavity base and along the horizontal boundaries between the two cells (figure 2*b*).

With continued solidification, additional double-diffusive cells are generated at the top and bottom of the stratified zone at the base of the cavity in regions where the accumulation of solute-enriched liquid is most pronounced. In figure 2(*c*), for example, taken after 40 minutes, two horizontal convection cells are visible near the base of the cavity and the main thermal cell has become restricted to the upper approximately 75% of the liquid region. Figure 2(*d*, *e*) shows photographs of the system at approximately 40 and 70% solidification, showing two or three, and (at least) six cells, respectively, within the density-stratified liquid at the base.

The form and behaviour of these secondary cells is similar to the convective patterns observed during lateral heating of an established salinity gradient (e.g. Chen 1974). The current system differs from these classical examples of double-diffusion in that the vertical solute gradient, which develops as a result of solidification, is nonlinear, and varies in magnitude and extent during the course of solidification. The nature of the compositional boundary layer along the solid/liquid interface controls the distribution of solute in the lower zone, which in turn determines the manner in which additional double-diffusive cells develop. In contrast to the experiments between impermeable boundaries, the double-diffusive cells are generated in a sequential fashion, on top of, and along the boundaries between, existing cells.

In the aqueous system investigated here, the macroscopic shape of the solid/liquid boundary is controlled primarily by convective heat transfer in the solution in the vicinity of the crystallization front. As the cavity is solidified and the density-stratified layer is established at the base, the circulation patterns in the liquid change, producing a continuous evolution in the thermal conditions perpendicular to the moving phase boundary. In the density-stratified portion of the liquid at the base of the cavity, the vigour of convective motion is reduced in comparison to that in the overlying homogeneous portion of the liquid. As a result, the dominant mode of lateral heat transfer in the lower region where the cells have formed is by conduction, and the solidification interface is nearly vertical. In the upper regions of the cavity, heat transfer is controlled by the vigorous thermal convection and the solid/liquid interface develops a shape that is typical of phase change in the presence of natural convection in the melt (Szekely & Chabbra 1970; Albert & O'Neill 1985; Morgan 1981).

The surface of the ice block remained smooth throughout most of the solidification interval, with little or no evidence of the onset of morphological instability, or the development of a pronounced dendritic or 'mushy' region. However, closer examination of the ice surface revealed a very tightly packed array of fine-scale

dendrites in a zone approximately 1–2 mm thick (porosity estimated at less than 5%, dendrite arm spacings on the order of 0.1 mm). The development of the morphological instability was only evident during the later stages of solidification.

The nature of the ice front observed in these experiments can be compared to what has been observed previously when solutions with initial compositions on the sodium carbonate-rich side of the eutectic (hypereutectic) are solidified under similar conditions (Chen & Turner 1980; McBirney 1980; McBirney *et al.* 1985; Thompson 1986; Turner & Gustafson 1981). In these experiments with hypereutectic solidification, a dendritic region on the order of 1 cm wide, characterized by dendrite arm spacings on the order of 0.1–2 mm (depending on the solidification conditions), is present between the (100%) liquid and solid (hydrated sodium carbonate) phase.

The existence of a mushy region is neglected in the theoretical analysis of §3, owing to the additional complexity and prohibitive computation time that is involved in incorporating a third solution region into the mathematical formulation. Furthermore, the assumption of a 'planar' phase boundary used to develop the mathematical formulation is consistent with the restricted width and low porosity of the mushy zone observed experimentally with hypereutectic solidification.

Figure 3(*a*, *b*) shows photographs of a similar experiment in which the heat input into the vertical wall was negligible. The main convection cell recedes higher into the cavity with time, but the horizontal cellular motion, which was observed in the lower regions of the cavity during the previous experiments, is lacking. Solute-rich liquid continues to accumulate at the base of the cavity, creating a stable vertical solute gradient in the lower portion of the liquid, but the lateral temperature difference is insufficient to initiate double-diffusive motions. As a result, a nearly stagnant, density-stratified region develops below the thermal convection cell, increasing in vertical extent as solidification progresses.

The fluid circulation patterns that develop within the density-stratified region at the base of the cavity are controlled primarily by the thermal conditions at the heated wall. When the heat input is negligible, as in the second experiment described above, the density stratification stabilizes the liquid and convective motion is essentially damped. In contrast, when the left wall is heated, the stratified portion of the liquid circulates in slowly rotating horizontal layers or cells.

The behaviour of the solidifying sodium carbonate solutions is consistent with previous analytical and experimental studies of the stability of a linearly salinity-stratified layer of fluid that is heated or cooled through an impermeable vertical wall (Thorpe *et al.* 1969; *Chen et al.* 1971; Hart 1971). The experiments and stability analyses indicate that there exists a critical thermal Rayleigh number, based on the temperature difference between the hot and cold vertical walls, beyond which viscous forces are overcome, and the initially stagnant fluid convects spontaneously in a series of horizontal 'double-diffusive layers'.

The depth of these layers h is observed to scale with l, the distance a fluid element can rise in a given vertical salinity gradient $(\partial S/\partial z)$ to become 'neutrally buoyant':

$$l = \frac{\beta_T \Delta T}{\beta_S (\mathrm{d}S/\mathrm{d}z)_0} \approx 0.0375 \frac{\Delta T}{(\mathrm{d}S/\mathrm{d}z)_0}.$$

z is the dimensionless vertical distance z'/L, where L is the characteristic cavity dimension; ΔT is the reference temperature drop; and β_S and β_T are given in table 1. A prime denotes a dimensional quantity.

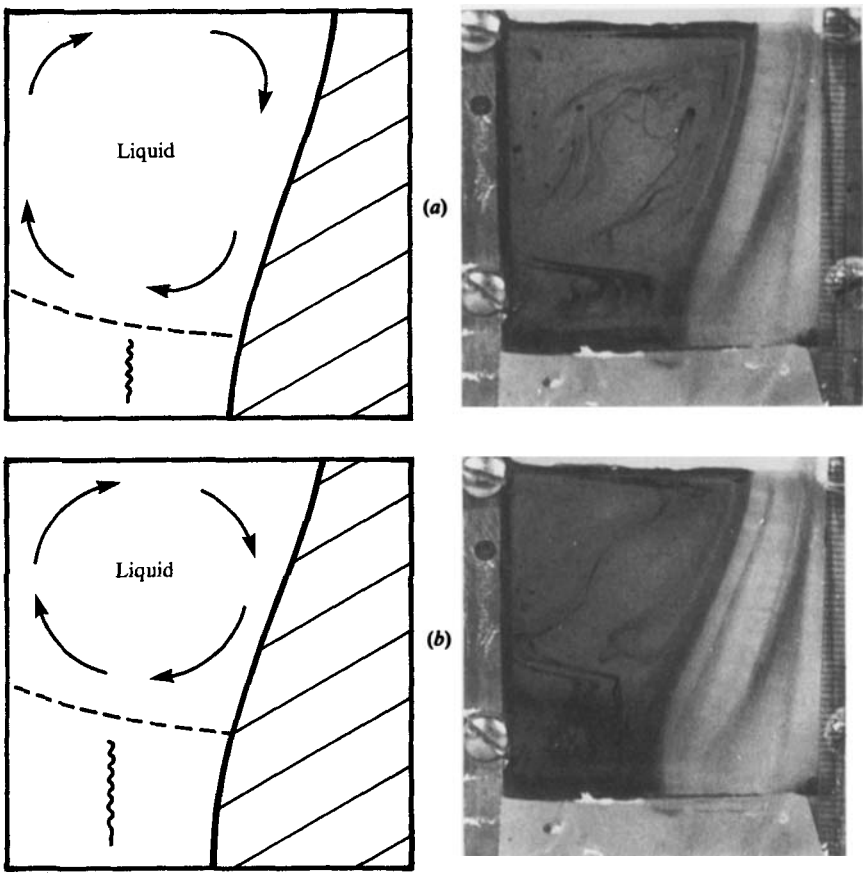

FIGURE 3. Photographs of a similar experiment in which the pumping rate through heated boundary was reduced. The horizontal thermal gradients are insufficient to destabilize the stable vertical solute gradient ($R_T < R_c$) and the stratified zone remains essentially stagnant. (*a*) After 25 min the stagnant region occupies the lower $\sim 0.25\%$ of the liquid region, but there is no evidence of double-diffusive layers at the base. (*b*) After 45 min additional dense liquid has accumulated beneath the thermal convection cell, but the fluid motion in the lower region is almost negligible.

Here the solute concentration

$$S = \frac{S' - S^{\mathrm{R}}}{\Delta S},$$

with S^{R} the reference solute concentration and ΔS the reference composition change.

Using l as the vertical lengthscale to evaluate the thermal Rayleigh number, the critical value at the onset of spontaneous cell generation was determined to be $1.5 \times 10^4 \pm 2500$ (Chen *et al.* 1971; Chen 1974; Hart 1971; Thorpe *et al.* 1969).

In the experiments with aqueous sodium carbonate solutions described in this section, double-diffusive layering in the stratified zone occurs only when the horizontal thermal gradient exceeds a minimum value, suggesting that the system is governed by stability criteria analagous to those for double-diffusion between impermeable boundaries. For the first experiment, the thermal gradient exceeded the critical value and double-diffusive layers were initiated. In contrast, during the second experiment, the magnitude of the thermal Rayleigh number was apparently

	Definition	Value for Na_2CO_3-H_2O System
ρ	density	1.0 g $(cm^3)^{-1}$ (15 wt % Na_2CO_3) 1.16 g $(cm^{3-1}$ (0 wt % Na_2CO_3)
κ	thermal diffusivity	1.5×10^{-3} cm^2/s (liquid) 1.5×10^{-3} cm^2/s (solid)
k	thermal conductivity	1×10^{-3} cal/cm s °C (liquid) 1×10^{-3} cal/cm s °C (solid)
ΔH	latent heat of fusion	76.0 cal/g
ν	kinematic viscosity	0.93×10^{-2} cm^2/s
D	solute diffusivity	1.5×10^{-5} cm^2/s
β_T	coefficient of thermal expansion	3.0×10^{-4} $°C^{-1}$
β_S	coefficient of solutal expansion	8.0×10^{-3} $wt\,\%^{-1}$
m'	slope of liquidus line	−0.33 °C/wt %
k_D	distribution coefficient	0
L	characteristic length (average cell size)	5 cm
h	lengthscale for secondary cells	0.5 to 1.0 cm (advanced stage) (intermediate)
$\sigma = \frac{\nu}{\kappa}$	Prandtl number	6.0
$Le = \frac{\kappa}{D}$	Lewis number	107.0
$R_T = \frac{g\beta_T \Delta T L^3}{\nu\kappa}$	Thermal Rayleigh number	5×10^5
$R_S = \frac{g\beta_S \Delta S L^3}{\nu\kappa}$	Solutal Rayleigh number	1×10^6
$St = \frac{\Delta H}{C_p \Delta T}$	Stefan number	5.0
$\gamma = \frac{\kappa_l}{\kappa_s}$	Ratio of thermal diffusivities of solid and liquid	1.0
$K = \frac{k_l}{k_s}$	Ratio of thermal conductivities of solid and liquid	1.0
$\Gamma = \frac{\beta_T \Delta T}{\beta_S \Delta S}$	Buoyancy ratio	0.5
R_c	Critical Rayleigh number at onset of flow instability	1.5×10^4

TABLE 1. Physical constants and dimensionless quantities

below the critical value R_c' necessary for convective instability, and the fluid remained stagnant.

These observations are consistent with the conclusions of Huppert & Turner (1980) concerning the formation of double-diffusive layers adjacent to a vertical ice wall melting into a linearly stratified layer of salt water. The authors demonstrated that the formation and behaviour of double-diffusive layers at the ice front could be analysed in a manner analagous to that used for heated or cooled impermeable boundaries. The primary difference between their experiments and those involving

impermeable walls is that the melting ice wall is immersed in a relatively wide tank for which the appropriate characteristic horizontal temperature drop is:

$$\Delta T_{\mathrm{H}} = T_{\infty} - T_{\mathrm{wall}}.$$

where T_{∞} is the far-field liquid temperature and T_{wall} is the temperature of the melting ice surface. For both the ice surface and impermeable walls, the measured thickness of the convecting layers h, for a wide range of the thermal Rayleigh number R_T, has been shown to scale with l according to:

$$h = c \times l$$

(Chen *et al.* 1971; Wirtz *et al.* 1972; Huppert & Turner 1980). The value of c is observed to decrease from approximately 1 to 0.66 as the thermal Rayleigh number is increased beyond R_{c} to 5×10^5, whereafter c remains essentially constant.

In the current experiments, the vertical salinity gradient in the bulk is neither constant with time nor necessarily linear in space, so that layer size h varies with height and changes throughout the course of solidification. As a result it is difficult to define a straightforward relationship between the layer size and R_T without extensive measurements of T_z and S_z. For this reason, there has been no effort in this investigation to systematically determine cell size variation or to define the stability criterion for the generation of convecting layers. However, the system studied here is very similar to that used by Huppert & Turner (1980), so that it is reasonable to apply the same principles established by these authors, in an approximate manner, to the analysis of the current set of experiments.

3. Analysis

The experiments of the previous section describe the progressive density stratification of a uniform fluid, and the concurrent development of double-diffusive instabilities within the liquid, which occur during horizontal solidification. In the following we develop a two-dimensional mathematical model of the solidification process for a binary, double-diffusive liquid in an enclosed cavity. The purpose of the modelling is to provide a quantitative description of the behaviour of the experimental system that will provide insight into the mechanism of generation of the double-diffusive instabilities.

The geometry chosen for the analysis is shown in figure 4. A binary fluid, initially homogeneous in composition and temperature, is confined to a two-dimensional square cavity and solidified directionally. The bounding walls of the cavity are impermeable and the top and base are thermally insulated.

At a time $t = 0$, where $t = t'\kappa/L^2 = t'/\tau$ is the dimensionless time (κ being thermal diffusivity), the vertical boundaries are raised/lowered to temperatures of $\theta_{\mathrm{H}}/\theta_{\mathrm{C}}$, and solidification proceeds inwards from the cold wall of the cavity. Here $\theta = (T' - T^0)/\Delta T'$ is the dimensional temperature, T^0 being the initial temperature. The solid phase differs in composition from the bulk liquid, causing the rejected solute to be concentrated in the liquid in the vicinity of the solid/liquid interface. The lateral temperature and solute concentration gradients that develop during solidification contribute to a thermosolutal buoyancy force which produces convective motions in the liquid. The density of the liquid is given, as a function of both solute concentration and temperature, by a linear equation of state of the form

$$\rho = \rho^0\{1 - \beta_T(T' - T^0) + \beta_S(S' - S^0)\}. \tag{1}$$

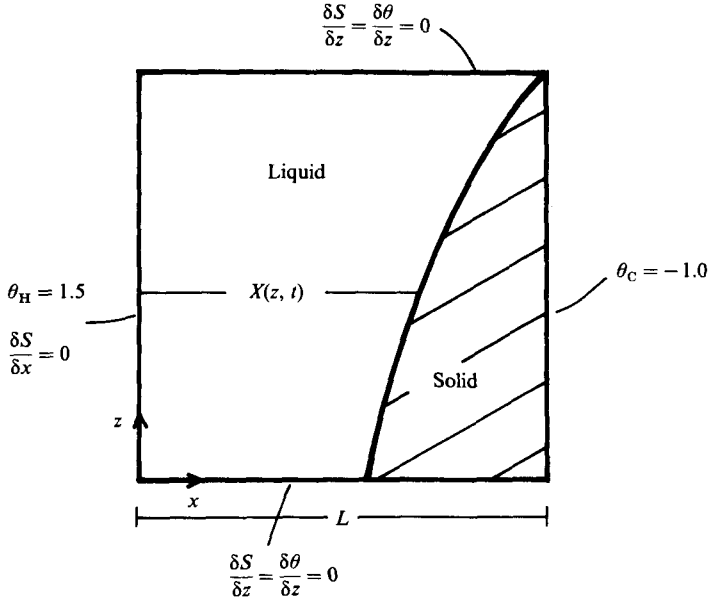

FIGURE 4. Schematic diagram of the system upon which the mathematical model is based. A homogeneous binary fluid is confined to a two-dimensional square cavity with the boundary conditions as shown, and solidified against the cold vertical boundary.

The dimensionless form of the equations governing conservation of energy, mass and momentum in a constant-property fluid, subject to the Boussinesq approximation are

$$\frac{1}{\sigma}\frac{\mathrm{D}\omega}{\mathrm{D}t} = \nabla^2\omega + (R_T \nabla\theta^1_x - R_S \nabla S_x), \tag{2}$$

$$\nabla^2 \Psi = -\omega, \tag{3}$$

$$\frac{\mathrm{D}\theta^1}{\mathrm{D}t} = \nabla^2\theta^1, \tag{4}$$

$$\frac{\mathrm{D}S}{\mathrm{D}t} = (Le)^{-1}\nabla^2 S. \tag{5}$$

Here

$$\frac{\mathrm{D}\partial\langle\,\rangle}{\mathrm{D}t} = \frac{\partial\langle\,\rangle}{\partial t} + u\frac{1}{\delta}\left(\frac{\partial\langle\,\rangle}{\partial x}\right) + v\left(\frac{\partial\langle\,\rangle}{\partial z}\right),$$

$$\nabla^2\langle\,\rangle = \frac{1}{\delta^2}\left(\frac{\partial^2\langle\,\rangle}{\partial x^2}\right) + \left(\frac{\partial^2\langle\,\rangle}{\partial z^2}\right) \qquad \text{liquid region,}$$

$$\nabla^2\langle\,\rangle = \frac{1}{(1-\delta)^2}\left(\frac{\partial^2\langle\,\rangle}{\partial x^2}\right) + \left(\frac{\partial^2\langle\,\rangle}{\partial z^2}\right) \qquad \text{solid region,}$$

$$\nabla\langle\,\rangle_x = \frac{1}{\delta}\left(\frac{\partial\langle\,\rangle}{\partial x}\right) \qquad \text{liquid region,}$$

$$\nabla\langle\,\rangle_x = \frac{1}{(1-\delta)}\left(\frac{\partial\langle\,\rangle}{\partial x}\right) \qquad \text{solid region,}$$

The dimensionless horizontal distance is defined as:

$$x = \frac{x'}{X(z,t)} \qquad \text{in the liquid region,}$$

and

$$x = \frac{x' - X\{z,t\}}{L - X\{z,t\}} \qquad \text{in the solid region.}$$

The dimensionless vorticity $\omega = \omega' L^2/\kappa$; and $\Psi = \Psi'/\kappa$ is the dimensionless stream function. The dimensionless horizonal velocity $u = u'L/\kappa$ and the dimensionless vertical velocity $v = v'h/\kappa = v/\vartheta$. The Lewis number Le and the thermal Rayleigh number R_T are given in table 1; and $\delta = X'(t,z)/L$ is the relative width of liquid.

In the solid phase, diffusion of solute is assumed negligible and conservation of energy requires

$$\frac{\partial \theta^s}{\partial t} = \gamma \nabla^2 \theta^s \tag{6}$$

where superscripts s, l refer to solid and liquid phases respectively, and γ is the ratio of thermal diffusivities of solid and liquid κ_l/κ_s.

The boundary conditions for a square cavity of dimension L are

$$\nabla\theta^l_z = \nabla S_z = u = v = 0 \quad (0 < x < L; \quad z = 0, L), \tag{7}$$

$$\left.\begin{aligned} \theta^l &= 1.5 \\ \nabla S_x &= u = v = 0 \end{aligned}\right\} \quad (x = 0; \quad 0 < z < L), \tag{8}$$

$$\theta^s = -1.0 \qquad (x = L; \quad 0 < z < L), \tag{9}$$

where x and z refer to horizontal and vertical directions respectively. At the phase boundary $\{x = X(z,t)\}$, conservation of energy and mass require that

$$(K\nabla\theta^s_x - \nabla\theta^l_x) f = St \frac{\partial \delta}{\partial t}, \tag{10}$$

$$\nabla S_x f = Le\, S^* (k_D - 1) \frac{\partial \delta}{\partial t}, \tag{11}$$

where $f = 1 + (\partial\delta/\partial z)^2$ is the shape factor, and k_D is the distribution coefficient. The particular form of f used here implies that the vertical variation of temperature and equilibrium solute concentration at the solid–liquid boundary is small or that

$$\boldsymbol{n}_t \cdot \nabla S \sim \boldsymbol{n}_t \cdot \nabla T \sim 0,$$

where $\boldsymbol{n}_t$ is the tangent vector at the boundary. The use of this approximate expression for f is valid here because, although the interior of the fluid is thermally and solutally stratified, the vertical variations at the solid/liquid boundary are quite small (< 2 °C over the cavity height). A similar approach has been successfully adopted by previous authors examining solidification in binary alloys (Brown *et al.* 1984).

The interface temperature θ^* and solute concentration S^* are related by the dimensionless slope of the liquidus m according to

$$\theta^* = \theta_{mp} + mS^*, \tag{12}$$

where θ_{mp} is the melting point of the pure solvent.

This system of coupled, nonlinear equations and boundary conditions describes

transient phase change in two dimensions. Most finite-difference schemes for handling this class of transport-phenomena problem (simultaneous heat, mass and momentum transfer), are designed for rectangular computational grids, and are therefore poorly suited to handle an irregular interface such as the solid–liquid boundary. For this reason, the governing equations are rewritten in a new coordinate system in which the solution domain is represented in terms of a more tractable geometric shape. The solidification problem of interest here involves only a single moving phase boundary, so that the Landau boundary immobilization technique has been chosen (Saitoh 1978; Hsu, Sparrow & Patankar 1981; Ramachandran & Gupta 1981; Gadgil & Gobin 1984; Sparrow, Patankar & Ramadhyani 1977; Ho & Viskanta 1984).

At each time-step, the irregularly shaped liquid and solid regions are transformed into rectangular domains for which specifying the boundary conditions is relatively straightforward. In transformed space the horizontal coordinate x in the liquid,

$$x = \frac{x^*}{X'(z,t)},$$

given in terms of the spatial coordinate in physical space $\{x^*\}$ and the width of the liquid region $\{X'\}$, ranges from 0 to 1 for all z and t. The advantage to this approach is that the solid/liquid boundary in transformed space is stationary, and defined by the position $x = 1$ during any given time interval.

In obtaining the final form of (2)–(6) and boundary conditions (7)–(12) in the adjusted coordinate system, a number of simplifying assumptions have been made. The first of these concerns the relative rates of solidification and convection. In systems with large (> 1) Stefan numbers (table 1), for which the interface velocity is slow relative to the fluid velocity, it is possible to adopt the 'quasi-stationary' approximation. The use of this approximation implies that over a limited time interval, the effect of interface motion on the temperature, solute and flow fields in the melt is negligible. The terms containing $\partial X'/\partial t$ can be therefore eliminated from the governing equations when solving for the velocity, temperature and solute concentration within the melt and solid. Sparrow *et al.* (1977), Ho & Viskanta (1984), Ramachandran *et al.* (1981), and Hsu *et al.* (1981) have demonstrated that the quasi-stationary approximation is valid for most phase-change problems with natural convection at moderate and large Stefan numbers.

The second assumption that has been made in the coordinate transformation is that the thickness of the melt region ($X'(z,t)$) varies slowly with z, so that terms involving $\partial X'/\partial z$ in the transport equations can be neglected. Ramachandran *et al.* (1981) and Ho & Viskanta (1984), have shown that this simplification is valid in systems as long as the vertical heat transfer across the upper and/or lower surfaces of the liquid and solid regions is not extreme. In fact, these authors have successfully used the same system of transformed equations as presented above in the solution of phase-change problems characterized by substantial radiative and convective heat losses along the upper surface of the cavity. The use of the 'interface-curvature' approximation is clearly even more appropriate for the current problem, in which the thermally insulated upper and lower boundaries of the enclosure ensure minimal heat loss through those surfaces.

The motivation for adopting this simplified form of the governing equations (with the 'quasi-stationary' and 'interface-curvature' approximations), is to reduce computation time and to ensure rapid convergence and stability in the solution procedure. The use of the quasi-stationary and interface-curvature approximations

for this particular moving-boundary problem is believed to be justified because of the magnitude of the Stefan number and the nature of the thermal boundary conditions at the horizontal boundaries. Select test cases of the numerical procedure, described elsewhere (Thompson 1986), have been used to verify the validity of these approximations as applied to this particular phase-change system.

The tranformed partial differential equations (2)–(6) and boundary conditions (7)–(12), are placed in finite-difference form using centred spatial derivatives for the diffusion terms, upwind differencing (Roache 1972) for the convective terms and forward time derivatives. The parabolic equations are solved implicitly using the standard Alternating-Direction-Implicit (ADI) technique, introduced by Peaceman & Rachford (1955), while the elliptic stream-function equation is solved iteratively using the method of Successive Overrelaxation (SOR) (Roache 1972). The nonlinearities in the convective terms and coupling between various equations and boundary conditions are handled iteratively.

Iteration at a specific time-step is continued until the maximum field residuals are reduced to 1×10^{-3}. Variable grid spacing in the horizontal direction has been used to facilitate computation at high Lewis numbers and care has been taken to place four to five grid points within the estimated width of the concentration boundary layer. Further details of the numerical scheme, including test cases and a more detailed discussion of convergence, stability and computation time are provided elsewhere (Thompson 1986).

The results presented in this section have been computed on the basis of the dimensionless quantities in table 2 which correspond to the physical parameters of the sodium carbonate–water solutions used in the experiments. The plotted results are given in terms of dimensionless parameters and variables, in order that they can be extrapolated to containers of any size (within the limits of the laminar flow regime), wall temperatures, etc., and to fluids with a range of physical parameters. The time comparisons are made in terms of a timescale

$$\tau \sim 1 \times 10^3 \text{ s} \sim 136 \text{ min}$$

using the average height of the main thermal convection cell (3.5 cm) as the lengthscale for the solidification process.

Figure 5(*a–c*) represents the stream function, solute concentration and temperature distributions within the cavity calculated on a 31 (x) by 51 (z) grid at a dimensionless time of 0.1 (13.6 min). During the early stages of solidification the fluid circulates in a single convection cell, driven primarily by the horizontal thermal gradients. The effect of the solute concentration on the liquid density is already apparent. The streamlines are concentrated in the region adjacent to the solid/liquid interface where the horizontal solute and temperature gradients have a reinforcing effect on the buoyancy force.

The temperature distribution (figure 5*b*) is characterized by large temperature gradients near the vertical boundaries and a stable, thermally stratified, core region. The shape of the solid/liquid interface reflects the pattern of convective heat transfer in the liquid region with the width of the solidified region reaching a maximum at the base where the thermal boundary layer is thickest. Convection is the primary mechanism responsible for the transport of rejected solute along the phase boundary towards the base of the cavity where the solute-rich liquid accumulates during solidification (figure 5*c*).

The vertical solute gradients, which result from this continued accumulation, contribute to the initiation of double-diffusive instabilities, which appear as multiple

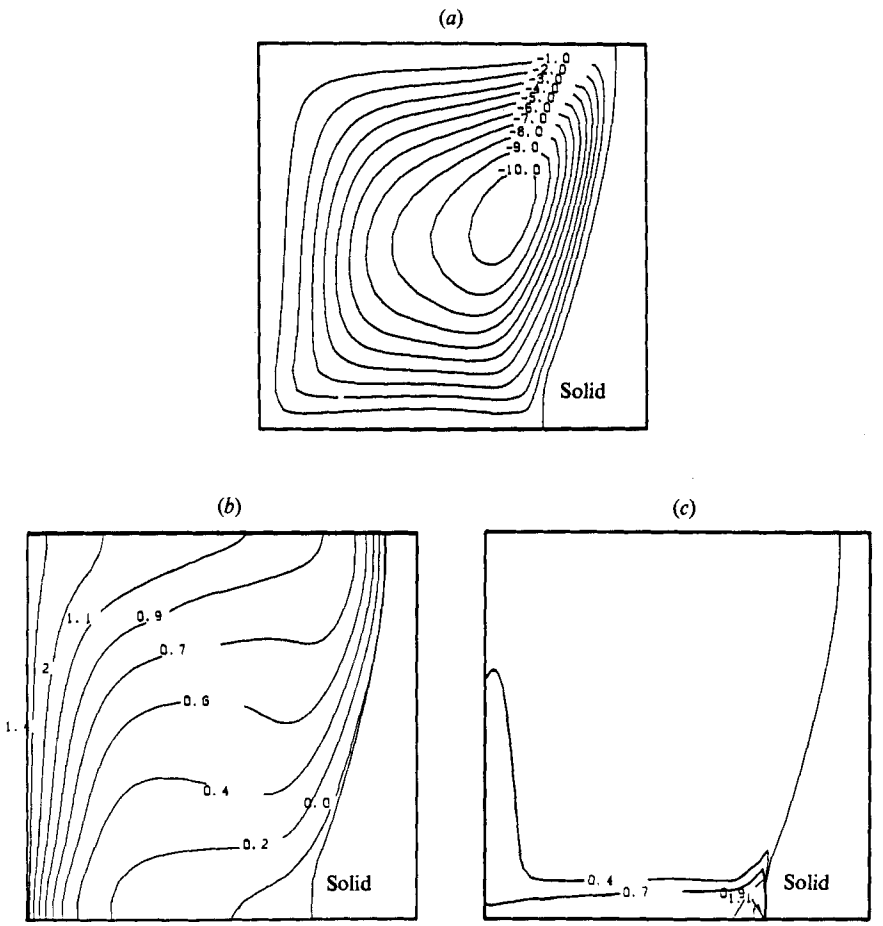

FIGURE 5. Contour plots of the calculated (*a*) stream function, (*b*) temperature and (*c*) solute concentration at a dimensionless time of 0.1 (13.6 min). The behaviour of the system at this stage is typical of solidification of a pure liquid, with the fluid motion confined to a single circulation loop.

convection loops within the density-stratified region. The first instability is generated at $t = 0.28$ (38 min), in the lower-left corner, and propagates across the cavity to form a horizontal double-diffusive convection cell beneath the main thermal convection cell (figure 6*a*). Within the upper cell the solute concentration is nearly uniform (figure 6*c*) and the isotherm distribution is typical of thermally driven natural convection in a pure liquid (figure 6*b*). In contrast, the lower cell exhibits steep vertical concentration gradients and more-nearly vertical isotherms, suggestive of low-Rayleigh-number convection in shallow cavities (Simpkins & Dudderar 1981).

At a dimensionless time of 0.3 there is evidence of the initiation of an additional double-diffusive instability between the main thermal cell and the low-aspect-ratio cell at the base. By $t = 0.32$ (43.5 min), two horizontal convection cells have become established beneath the main cell, with the horizontal boundaries between the cells tilting up slightly in the direction of the heated boundary (figure 7*a*). Convection within the upper cell is more vigorous, exhibiting maximum velocities two to three times higher than in the lower cells. At this time the solute stratification extends throughout the lower one-third of the cavity (figure 7*b*) and the convective mixing

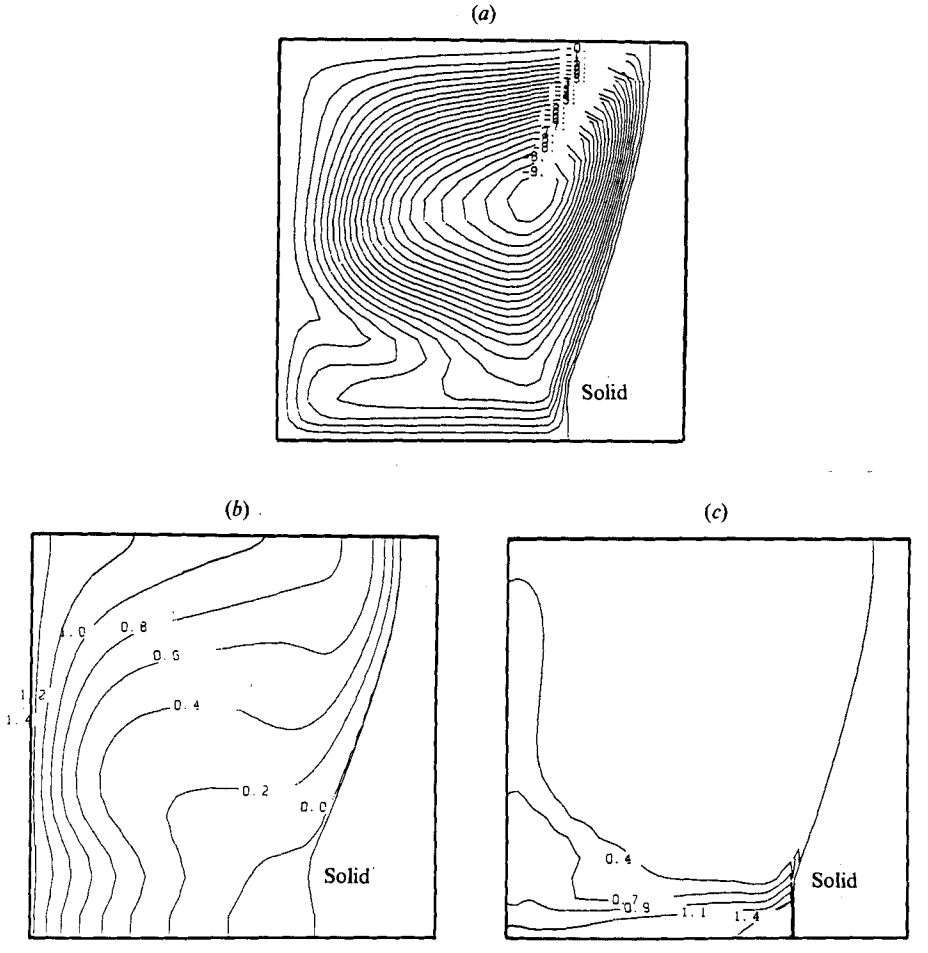

FIGURE 6. Contour plots of the calculated (*a*) stream function, (*b*) temperature and (*c*) solute concentration at a dimensionless time of 0.28 (38.2 min). The denser, solute-rich liquid accumulates near the base and the combination of the vertical solute gradient and the horizontal temperature gradient in the lower portion of the liquid leads to the formation of a double-diffusive layer beneath the thermal convection loop.

between the cells is limited. The main mechanism of heat and mass transfer between the separate convecting regions occurs by diffusion across the horizontal interfaces which separate them.

At a dimensionless time of 0.48 (65.2 min), the cavity is approximately 35% solidified (figure 8*a*) and the original thermal convection cell is restricted to the upper half of the cavity. Three to four slowly rotating double-diffusive cells are discernible within the lower half of the liquid where the vertical solute gradient is steepest (figure 8*b*). The circulation is slightly more vigorous within the lowest two double-diffusive cells than in the central region of the liquid, apparently owing to the presence of the (solid) cavity base. The cellular motion near the base acts to perturb the isotherms slightly (figure 8*c*) and initiate the development of a vertically layered solute distribution (figure 8*d*).

The influence of the double-diffusive layering on the development of vertical

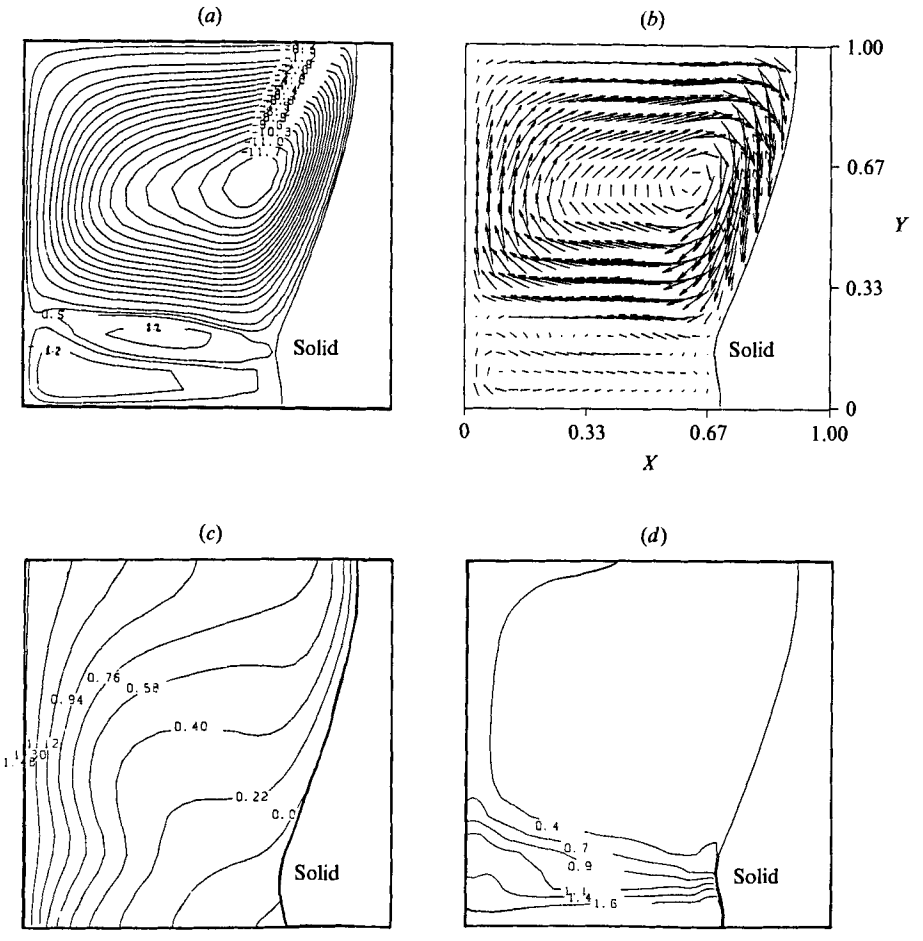

FIGURE 7. Contour plots of the calculated (*a*) stream function, (*b*) velocity vector, (*c*) temperature and (*d*) solute concentration at a dimensionless time of 0.32 (43.5 min). Two low-aspect-ratio double-diffusive convection layers have formed at the base of the cavity, exhibiting the same direction of circulation, but lower convective velocities, than the overlying thermal-convection cell.

stratification in the interior of the cavity is evident from the vertical profiles of dimensionless temperature, solute concentration and 'density', defined as

$$\rho = \left| 1 - \frac{R_S S - R_T \theta}{R_T \theta} \right|$$

of figure 9(*a–c*). At the time the first double-diffusive layer forms at the base of the cavity, the overall vertical thermal and compositional zoning in the bulk liquid has become well established (figure 9*a* – corresponding to contour plots of figure 6). The solute concentration in the liquid of the overlying thermally convecting region is approximately uniform, but increases dramatically at the level of the first front and is nearly uniform within the double-diffusive layer. In contrast, the upper region is characterized by a pronounced thermal gradient, with temperature increasing gradually from base to roof of the cavity, as is typically observed in thermal natural convection in enclosures.

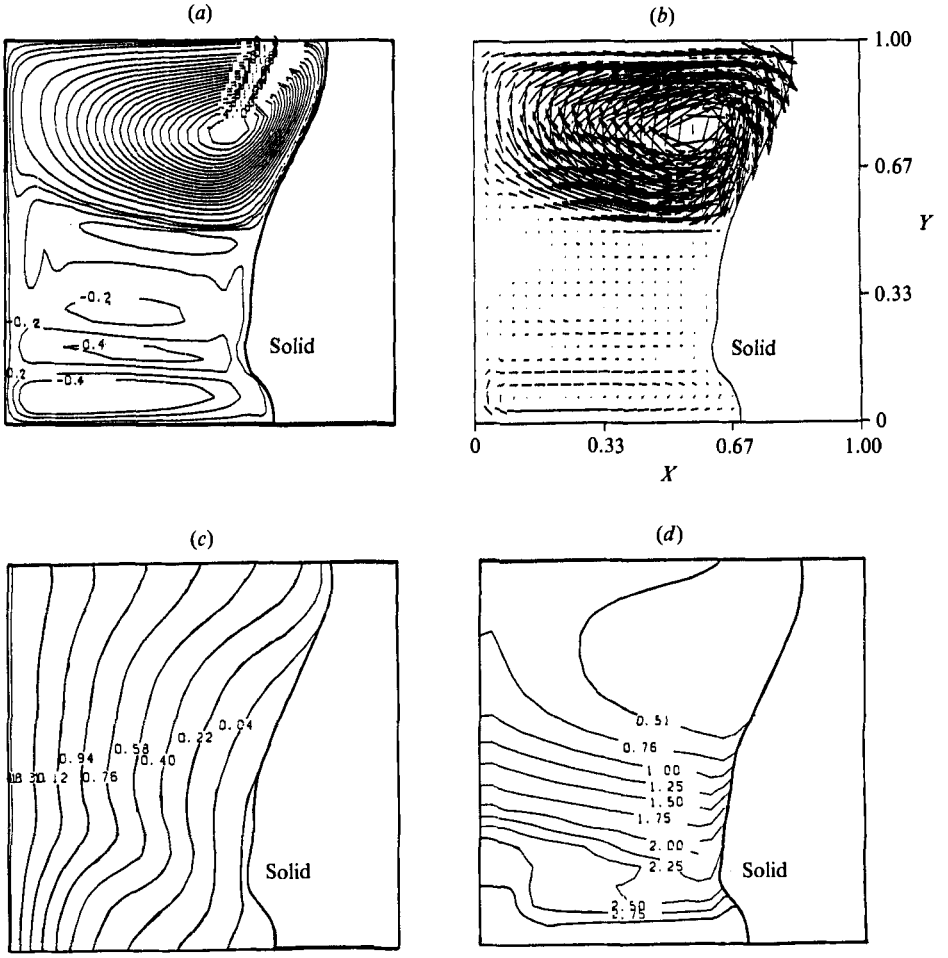

FIGURE 8. Contour plots of the calculated (*a*) stream function, (*b*) velocity vector, (*c*) temperature and (*d*) solute concentration at a dimensionless time of 0.48 (65.2 min). The thermal-convection cell is restricted to the upper half of the liquid region and there is evidence of between two and four double-diffusive layers forming near the base. The convection is slightly more vigorous in the lowest two layers than in the stagnant region in the central portion of the cavity.

After two double-diffusive layers develop (figure 9*b* – corresponding to figure 7), convection of the fluid above the first front is somewhat damped and the vertical thermal gradient in that region is correspondingly reduced. In the lower region, where the double-diffusive layers form, the vertical profiles show the step-like stratification characteristics commonly associated with thermohaline circulation. The profiles of figure 9(*c*) exhibit similar trends, with the thermal cell occupying the upper half of the liquid region and four double-diffusive layers present below the first front.

The shape of the solid/liquid boundary, at this time, reflects the competition between the compositional dependence of the melting temperature and the pattern of convecture heat transfer along the phase boundary. The maximum rate of solidification no longer occurs at the base of the cavity, but at a height that corresponds roughly to the base of the main convection cell, where heat transfer

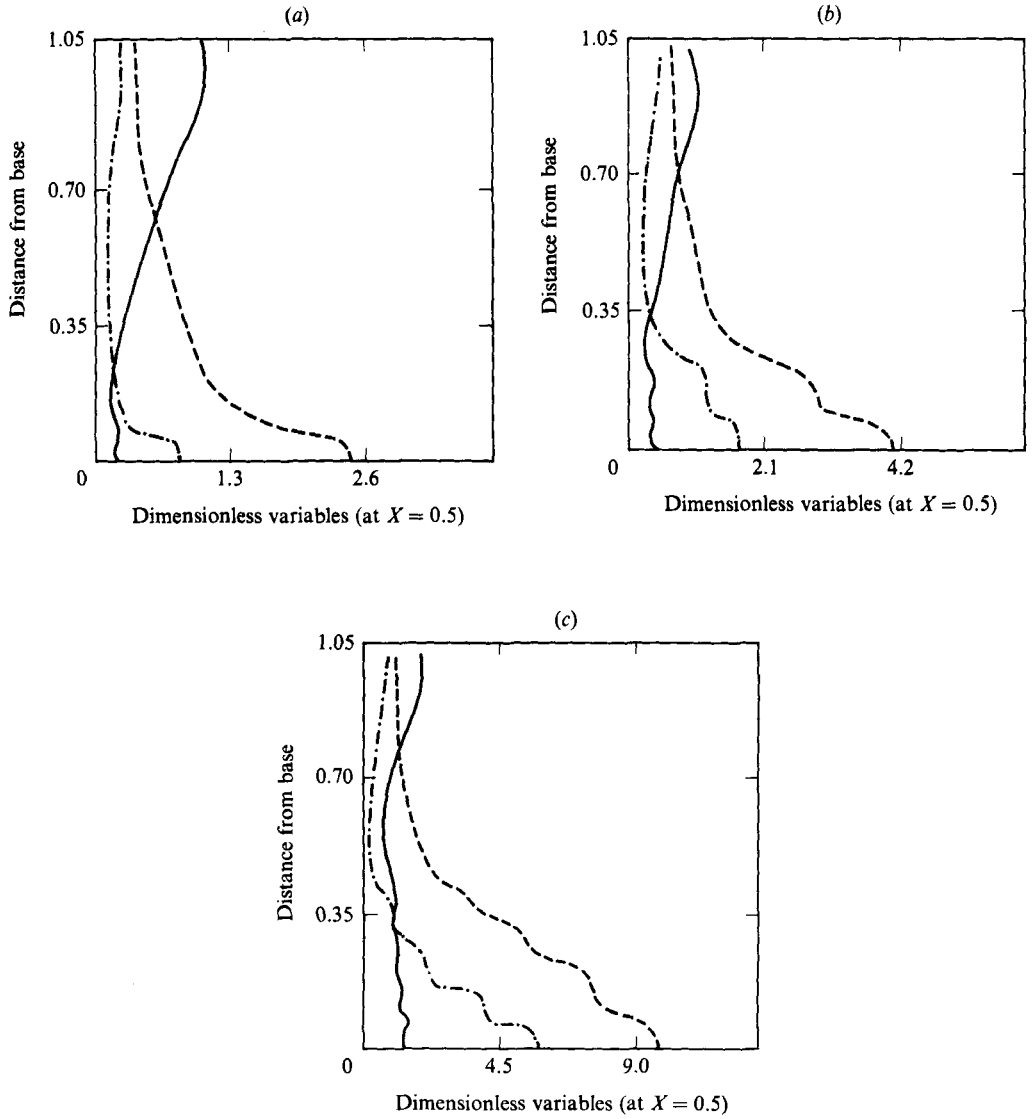

FIGURE 9. Vertical profiles of dimensionless solute concentration, temperature and liquid 'density' at $x = 0.5$ calculated at dimensionless times: (*a*) 0.28, (*b*) 0.32 and (*c*) 0.48. ——, temperature; –·–·–, solute concentration; – – –, density.

away from the interface is most efficient. Below this level, the increase in solute concentration and associated decrease in melting temperature results in a decreased solidification rate which is reflected in the shape of the phase boundary (figure 8).

The timescale associated with cell formation is much less than that associated with the solidification process, making it necessary to employ small time-steps in the calculations ($\Delta t = 0.0001$). For this reason, it has only been possible to compute flow fields for a limited portion of the solidification process. Nonetheless, there is very good agreement between the observed flow patterns and solidification behaviour and the predictions of the numerical calculations for the time period that has been investigated.

Order-of-magnitude analysis

Analysis of the velocity and length scales appropriate for natural convection provides additional insight into the expected behaviour of the system and allows the generalization of the findings reported here to a broader range of operating parameters. During the early stages of solidification, the behaviour of the system is similar to what is observed for thermally driven buoyancy flows. The relevant lengthscales appropriate for the experimental system are (Patterson & Imberger 1980)

$$\delta_T \sim \frac{L}{R_T^{\frac{1}{4}}} \sim 0.15 \text{ cm},$$

$$\delta_V \sim \sigma^{0.5}\,\delta_T \sim 0.5 \text{ cm},$$

$$\delta_c \sim Sc^{-0.33}\,\delta_V \sim 0.05 \text{ cm},$$

where subscripts T, V, c refer to thermal, viscous and concentration, respectively.

The vertical boundary-layer flow has a characteristic velocity of order

$$V \sim \frac{R_T^{0.5}\,\kappa^1}{L} \sim 18 \text{ cm/min}$$

($L = 5$ cm, $R_T = 1 \times 10^6$, $\kappa = 1.5 \times 10^{-3}$ cm^2/s), while the horizontal intrusion layers at the base and top of the cavity of thickness

$$\Delta \sim \frac{L}{R_T^{\frac{1}{4}}\,\sigma^{\frac{1}{3}}} \sim 0.2 \text{ cm}$$

have velocities of order $$U \sim \frac{V\delta_T}{\Delta} \sim 14 \text{ cm/min}.$$

Once the double-diffusive cells are established near the base of the cavity, the convective behaviour within each cell is similar to what would be predicted for an individual (low-aspect-ratio) cavity of height h ($< L$). Assuming a lengthscale of 0.5 cm (the average cell height: e.g. figure 2*e*), appropriate for the advanced stages of solidification, the reduced velocities (V^* and U^*) estimated for the double-diffusive cellular convection are

$$V^* \sim 2 \text{ cm/min}, \quad U^* \sim 1.2 \text{ cm/min}.$$

In addition, the (experimental) convective velocities have been estimated from the rate of propagation of dye within the vertical and horizontal boundary layers. Table III lists the observed and calculated maximum convective velocities for various times during solidification. The comparisons have been based on a velocity scale of:

$$\vartheta \sim 3.0 \times 10^{-3} \text{ cm/s} \sim 0.18 \text{ cm/min}.$$

Again, the characteristic length used for scaling is the average height of the double-diffusive cells forming during the intermediate and advanced stages of solidification (0.5 cm). There is relatively good agreement between observed and calculated convective velocities as well as with the order-of-magnitude estimates outlined above. The calculated and experimental velocities for motion in the double-diffusive layers are also consistent with the results of Wirtz *et al.* (1972), who report velocities between 0.6 and 2.2 cm/min, increasing as R_T is increased beyond R_c.

Time	Estimated (experimental)	Calculated	
		Dimensionless	Dimensional
0.2	10–15 cm/min	86.1	15.5 cm/min
	5–8 cm/min (upper cell)	28.9	5.2 cm/min
0.3	1–2 cm/min (lower cell)	12.5	2.25 cm/min
	3–6 cm/min (upper cell)	20.8	3.75 cm/min
0.4	< 1 cm/min (lower cell)	3.6	0.5 cm/min

TABLE 2. Comparison of experimental and calculated convective velocities

The horizontal destabilizing force, which is responsible for the initiation of the layering ($\propto \Delta T$), is roughly uniform throughout the depth of the tank. In contrast the magnitude of the vertical stabilizing force, which is proportional to $\partial S/\partial z$, varies with height and is negligible within the homogeneous liquid of the upper convection cell. The lengthscale l, the thermal Rayleigh number based on that lengthscale, and the characteristic flow velocity therefore differ for the upper cell and the lower stratified region. As a result, as table 2 indicates, convection in the overlying thermal convection cell is characterized by somewhat higher velocities than evidenced in the horizontal double-diffusive layers.

In studies of double-diffusive layering in stratified solutions (Wirtz *et al.* 1972; Chen *et al.* 1972; Chen 1974; Huppert & Turner 1980) the lengthscale is defined in terms of the initial vertical salinity (solute) gradient in the fluid layer. For the current analysis of the experimental results, however, it is more appropriate to use the estimated solute gradient within the stratified zone at the base, to define the lengthscale h for that region of the liquid during a specific stage of solidification.

Furthermore, due to the relative proximity of the two 'vertical' solid surfaces, we have chosen to evaluate the horizontal thermal driving force in terms of the temperature difference between the heated wall and the solidification front (as used commonly for the analysis of layering in stratified solutions). For the stage portrayed in figure 2(*e*), in which the temperature and solute concentration at the interface approach the eutectic, we use as the horizontal temperature difference:

$$\Delta T \sim (T_{\mathrm{H}} - T_{\mathrm{eutectic}}) \sim 17\ ^{\circ}\mathrm{C},$$

and assume a difference in solute concentration within this stratified zone, of 4 wt % (between the initial and eutectic compositions) over a vertical distance of 3.5 cm. This leads to an estimated vertical solute concentration gradient of 1.14 wt %/cm and an estimated value of the lengthscale h of 0.56 cm. For comparison, the measured cell heights l (figure 2*e*) are between 0.4 and 0.6 cm, which agree with the values of (l/h) determined previously for impermeable boundaries (Chen 1974; Huppert & Turner 1981).

4. Discussion and conclusions

We have presented both computed and experimental results on double-diffusive phenomena arising during horizontal solidification of a binary, aqueous solution. The modelling describes the manner in which vertical concentration gradients develop in a homogeneous liquid as a result of convective redistribution of a denser solute rejected along a moving, solid/liquid interface.

The convective patterns that develop in the stratified liquid region are governed by the interaction of the horizontal thermal gradient with this vertical solute stratification. For values of the (horizontal) thermal Rayleigh number below a critical value R_c, the portion of the liquid region over which the solute stratification extends remains essentially stagnant throughout solidification. For solidification at higher Rayleigh numbers, the lateral temperature gradient is sufficient to destabilize the solute stratification, causing the formation of low-aspect-ratio (horizontal) double-diffusive cells within the growing, density-stratified region.

The average height of the double-diffusive cells is determined by the relative magnitude of the horizontal destabilizing and the (local) vertical stabilizing buoyancy forces (equation (13)), with larger horizontal thermal gradients resulting in the formation of fewer, and larger, double-diffusive cells within the same depth of fluid. If the thermal gradient is very large, relative to the vertical solute gradient, the density stratification will be suppressed owing to the tendency of the solute-rich liquid to remix with the homogeneous liquid of the thermal convection cell.

Although the general characteristics of cellular convection in this system appear to be governed by the same principles as control thermohaline convection between impermeable boundaries, the time-dependent behaviour of the system is somewhat more complex. The aspect ratio of the liquid region and the vertical extent and magnitude of the density stratification are continuously changing, so that the secondary double-diffusive cells are generated in a sequential fashion (rather than simultaneously), both above and below existing cells. Furthermore, the boundary-layer motion, which is known to have only a secondary influence on thermohaline convection, controls the manner in which the solute is transported from the growing crystals and redistributed within the interior. Therefore, the conditions along the solid/liquid boundary, including the rate of solidification, the nature of the interface and the horizontal gradients, influence the time-dependent behaviour of the system.

The preceeding analysis has focused upon the development of double-diffusive instabilities in an aqueous system, but the results can be considered in the broader context of solidification of multi-component magmatic systems, liquid metal alloys, and binary and ternary semiconductor materials. In all of these, the potential exists for the development of double-diffusive instabilities due to the interaction of temperature and solute concentration gradients that form as a result of solidification/melting. It is hoped that the mathematical modelling presented here can be extended to determine the conditions under which double-diffusive phenomena of this type may be important.

Although it is premature to speculate on the role of double-diffusive phenomena in these systems, it is possible to gain some insight into their expected behaviour by comparing the values of the relevant physical parameters to those of the aqueous systems investigated here. Generally speaking, the onset of cellular convection is favoured by low Lewis numbers ($\sim 10^2$) and strong solutal buoyancy effects (small Γ, large β_S), (Chen 1974; Thorpe *et al.* 1969; Hart 1971).

The value of the solutal expansion coefficient (β_S), is dependent on the specific alloy or system under consideration. In metallic alloys, for example, β_S can be as large as -4×10^{-2} wt %$^{-1}$ (S, Si in steel) to 2×10^{-3} (Mo in steel) (Fujii, Poirer & Flemings 1979) compared with the value of 8×10^{-3} wt %$^{-1}$ appropriate for the aqueous sodium carbonate system. It is therefore feasible that the buoyancy ratio Γ characteristic of certain metals processing operations falls in the range for which double-diffusive instabilities may be generated.

In contrast, the Lewis number is on the order of 10^3–10^5 for metallic liquids, and even larger for the common chemical components in complex magmatic liquids. It would appear that the effect of an increased Lewis number would be to reduce the width of the concentration boundary layer and possibly to suppress the development of the vertical stratification through its influence on the boundary-layer motion. The present analysis, however, assumes a planar solid/liquid interface, a condition that is not likely to be strictly applicable to many actual solidification systems. In contrast, most magmatic and metallic systems are characterized by a dendritic or 'mushy' region between the liquid and solid phases. The distance over which solute segregation occurs in the vicinity of the phase boundary in these systems is therefore substantially larger than the width of the compositional boundary layer predicted for a planar crystal front. It is possible that this would offset the influence of the increased Lewis number. This suggests that, under certain operating conditions, these systems will develop significant (vertical) solute stratification which can lead to the generation of double-diffusive instabilities and/or the formation of stagnant regions in the liquid.

Unfortunately, there has been little effort, until recently, to investigate double-diffusive processes in actual solidification processing operations and the available experimental data on the physical properties of these systems are limited. However, there is experimental evidence that this type of phenomenon may be important in systems other than the aqueous solutions considered here. For example, Hebditch & Hunt (1974), and Fisher & Hunt (1979) report experimental results on the horizontal solidification of Pb–Sn, Sn–Pb and Sn–Zn alloys, in which they determine the spatial distribution of solute in the solid and liquid phases at various stages of solidification.

Their results show the presence of pronounced vertical solute stratification within the quenched liquid phase, which is reflected in the compositional inhomogeneities in the solidified product as well as the shape of the solid/liquid interface. For the case of an Sn alloy containing 5 wt % Pb, the denser solute-enriched liquid accumulated at the base of the cavity, whereas for Sn in Pb and Zn in Sn, the solute was lighter and accumulated in the liquid near the roof of the cavity. Unfortunately it is not possible to determine from their data whether the density-stratified liquid remained stagnant or developed into a series of double-diffusive convection regions of the type observed in the aqueous solution considered here. However, it is clear that, owing to the double-diffusive properties of these alloys, horizontal solidification resulted in transformation of the homogeneous liquid into a stably stratified liquid with pronounced vertical compositional gradients.

We can conclude that the double-diffusive nature of the binary systems investigated here has a controlling influence on flow patterns, and heat and mass transfer in the liquid phase during horizontal solidification. Furthermore, it is likely that similar double-diffusive phenomena may occur during solidification of other non-aqueous solutions in which the liquid density varies with solute concentration. In materials processing operations these double-diffusive interactions can be expected to influence the solidification/crystallization process through their effect on

heat transfer and solute redistribution in the vicinity of the solid/liquid interface, and therefore will be important in determining the compositional and textural homogeneity of the solidified product.

REFERENCES

ALBERT, M. R. & O'NEILL, K. 1985 Transient two-dimensional phase change with convection using deforming finite elements. In *Computer Techniques in Heat Transfer*, vol. 1 (ed. R. W. Lewis). Swansea: Pineridge.

BAINES, W. D. & TURNER, J. S. 1969 Turbulent buoyant convection from a source in a confined region. *J. Fluid Mech.* **37**, 51–80.

BROWN, R. A., CHANG, C. J. & ADORNATO, P. J. 1984 Finite element analysis of directional solidification of dilute and concentrated binary alloys. In *Modeling of Casting and Welding Processes II* (ed. J. A. Danzig & J. T. Berry). AIME.

CHEN, C. F. 1974 Onset of cellular convection in a salinity gradient due to a lateral temperature gradient. *J. Fluid Mech.* **63**, 563–576.

CHEN, C. F., BRIGGS, D. G. & WIRTZ, R. A. 1971 Stability of thermal convection in a salinity gradient due to lateral heating. *Intl J. Heat Mass Transfer* **14**, 57–65.

CHEN, C. F. & TURNER, J. S. 1980 Crystallization in a double-diffusive system. *J. Geophys. Res.* **85**, 2573–2593.

CORIELL, S. R., CORDES, M. R. & BOETTINGER, W. J. 1980 Convective and interfacial instabilities during unidirectional solidification of a binary alloy. *J. Cryst. Growth* **49**, 13–28.

FISHER, K. M. & HUNT, J. D. 1979 Observations on the nature and extent of gravitational interdendritic fluid flow. *Sheffield Intl Conf. on Solidification and Casting*, vol. 193, pp. 325–333.

FUJII, T., POIRIER, D. R. & FLEMINGS, M. C. 1979 Macrosegregation in a multicomponent low alloy steel. *Metall. Trans.* B**00**, 331–339.

GADGIL, A. & GOBIN, D. 1984 Analysis of two-dimensional melting in rectangular enclosures in the presence of convection. *Trans. ASME* C: *J. Heat Transfer* **106**, 20–26.

HART, J. E. 1971 On sideways diffusive instability. *J. Fluid Mech.* **99**, 279–288.

HEBDITCH, D. J. & HUNT, J. D. 1974 Observations of ingot macrosegregation on model systems. *Metall. Trans.* A**5**, 1557–1564.

HO, C. J. & VISKANTA, R. 1984 Heat transfer during melting from an isothermal vertical wall. *Trans ASME C: J. Heat Transfer* **106**, 12–19.

HSU, C. F., SPARROW, E. M. & PATANKAR, S. V. 1981 Numerical solution of moving boundary problems by boundary immobilization and a control-volume-based finite difference scheme. *Intl J. Heat Mass Transfer* **24**, 1335–1343.

HUPPERT, H. E. & TURNER, J. S. 1980 Ice blocks melting into a salinity gradient. *J. Fluid Mech.* **100**, 367–384.

HUPPERT, H. E. & TURNER, J. S. 1981 Double-diffusive convection. *J. Fluid Mech.* **106**, 299–329.

MCBIRNEY, A. R. 1980 Mixing and unmixing of magmas. *J. Volcanol. Geotherm. Res.* **7**, 357–371.

MCBIRNEY, A. R. BAKER, B. & NILSON, R. H. 1985 Liquid fractionation. Part I: Basic principles and experimental simulations. *J. Volcanol. Geotherm. Res.* **24**, 1–24.

MCFADDEN, G. B., REHM, R. G., CORIELL, S. R., CHUCK, W. & MORRISH, K. A. 1984 Thermosolutal convection during directional solidification. *Metall. Trans.* A**15**, 2125–2135.

MORGAN, K. 1981 A numerical analysis of freezing and melting with convection. *Comp. Meth. Appl. Engng* **28**, 275–284.

PATTERSON, J. & IMBERGER, J. 1980 Unsteady natural convection in a rectangular cavity. *J. Fluid Mech.* **100**, 65–86.

PEACEMAN, D. W. & RACHFORD, H. H. 1955 The numerical solution of parabolic and elliptic differential equations. *J. Soc. Indust. Appl. Maths* **3**, 28–41.

RAMACHANDRAN, N. & GUPTA, J. P. 1981 Two-dimensional solidification with natural convection in the melt and convective and radiative boundary conditions. *Numer. Heat Transfer* **4**, 469–484.

ROACHE, P. J. 1972 *Computational Fluid Dynamics*. Albuquerque: Hermosa.

SAITOH, T. 1978 Numerical method for multidimensional freezing problems in arbitrary domains. *Trans. ASME.* C: *J. Heat Transfer* 100, 294–299.

SIMPKINS, P. G. & DUDDERAR, J. D. 1981 Convection in rectangular cavities with differentially heated end walls. *J. Fluid Mech.* **110**, 433–456.

SPARROW, E. M., PATANKAR, S. V. & RAMADHYANI, S. 1977 Analysis of melting in the presence of natural convection in the melt region. *Trans. ASME* C: *J. Heat Transfer* **99**, 520–526.

SZEKELY, J. & CHHABRA, P. S. 1970 The effect of natural convection on the shape and movement of the melt-solid interface in the controlled solidification of lead. *Metall. Trans.* **1**, 1195–1203.

THOMPSON, M. E. 1986 Double-diffusive phenomena in horizontally-solidified binary liquids. Ph.D. thesis, MIT.

THORPE, S. A., HUTT, P. K. & SOULSBY, R. 1969 The effect of horizontal gradients on thermohaline convection. *J. Fluid Mech.* **38**, 375–400.

TURNER, J. S. 1974 Double-diffusive phenomena. *Ann. Rev. Fluid Mech.* **6**, 37–56.

TURNER, J. S. 1979 *Buoyancy Effects in Fluids*. Cambridge University Press.

TURNER, J. S. 1980 A fluid dynamical model of differential and layering in magma chambers. *Nature* **285**, 213–215.

TURNER, J. S. & GUSTAFSON, L. B. 1981 Fluid motions and compositional gradients produced by crystallization or melting at vertical boundaries. *J. Volcanol. Geothorm. Res.* **11**, 93–125.

WIRTZ, R. A., BRIGGS, D. G. & CHEN, C. F. 1972 Physical and numerical experiments on layered convection in a density-stratified fluid. *Geophys. Fluid Dyn.* **3**, 265–288.